

Effect of actuating frequency on plasma assisted detonation initiation

Si-Yin Zhou(周思引), Xue-Ke Che(车学科), Di Wang(王迪), Wan-Sheng Bie(聂万胜)
Citation: Chin. Phys. B . 2018, 27(2): 025208. **doi:** 10.1088/1674-1056/27/2/025208

Journal homepage: http://cpb.iphy.ac.cn; http://iopscience.iop.org/cpb

What follows is a list of articles you may be interested in

---

lectric ignition energy evaluation and the energy distribution structure of energy released in electrostatic discharge process

Qingming Liu(刘庆明), Jinxiang Huang(黄金香), Huige Shao(邵惠阁), Yunming Zhang(张云明)
Chin. Phys. B . 2017, 26(10): 105202. **doi:** 10.1088/1674-1056/26/10/105202

Conversion of an atomic to a molecular argon ion and low pressure argon relaxation

M N Stankov, A P Jovanović, V Lj Marković, S N Stamenković
Chin. Phys. B . 2016, 25(1): 015204. **doi:** 10.1088/1674-1056/25/1/015204

Current-voltage characteristics of hydrogen DC plasma torches with different sizes in an external axial magnetic field

Ma Jie, Wen Guang-Dong, Su Bao-Gen, Yang Yi-Wen, Ren Qi-Long
Chin. Phys. B . 2015, 24(6): 065205. **doi:** 10.1088/1674-1056/24/6/065205

Growth of small diameter multi-walled carbon nanotubes by arc discharge process

K. T. Chaudhary, J. Ali, P. P. Yupapin
Chin. Phys. B . 2014, 23(3): 035203. **doi:** 10.1088/1674-1056/23/3/035203

Effect of pulsed bias on properties of ZrN/TiZrN films deposited by cathodic vacuum arc

Zhang Guo-Ping, Wang Xing-Quan, Lü Guo-Hua, Zhou Lan, Huang Jun, Chen Wei, Yang Si-Ze
Chin. Phys. B . 2013, 22(3): 035204. **doi:** 10.1088/1674-1056/22/3/035204

Effect of actuating frequency on plasma assisted detonation initiation*

Si-Yin Zhou(周思引)[1], Xue-Ke Che(车学科)[1,2], Di Wang(王迪)[1], and Wan-Sheng Nie(聂万胜)[1,†]

[1] *Space Engineering University, Beijing* 101416, *China*
[2] *Science and Technology on Scramjet Laboratory, Changsha* 410073, *China*

(Received 31 August 2017; revised manuscript received 13 November 2017; published online 5 January 2018)

Aiming at studying the influence of actuating frequency on plasma assisted detonation initiation by alternating current dielectric barrier discharge, a loosely coupled method is used to simulate the detonation initiation process of a hydrogen-oxygen mixture in a detonation tube at different actuating frequencies. Both the discharge products and the detonation forming process which is assisted by the plasma are analyzed. It is found that the patterns of the temporal and spatial distributions of discharge products in one cycle are not changed by the actuating frequency. However, the concentration of every species decreases as the actuating frequency rises, and atom O is the most sensitive to this variation, which is related to the decrease of discharge power. With respect to the reaction flow of the detonation tube, the deflagration-to-detonation transition (DDT) time and distance both increase as the actuating frequency rises, but the degree of effect on DDT development during flow field evolution is erratic. Generally, the actuating frequency affects none of the amplitude value of the pressure, temperature, species concentration of the flow field, and the combustion degree within the reaction zone.

Keywords: alternating current dielectric barrier discharge, plasma assisted detonation initiation, actuating frequency, deflagration to detonation, active particles

PACS: 52.77.–j, 52.80.–s, 52.65.–y, 47.40.Rs **DOI:** 10.1088/1674-1056/27/2/025208

1. Introduction

As a recent hotspot in the field of aerospace propulsion, plasma assisted combustion (PAC) technology has incalculable application prospects in scramjet engines, detonation engines, auto-mobile internal engines, etc.[1–5] Among the known discharge methods of generating plasmas, dielectric barrier discharge (DBD) is widely used for combustion control as it is able to effectively prevent an arc from forming, to operate in a wide pressure range, and has a low heat loss.[6–11] Except for the relatively early studies on the basic theory of PAC by DBD, most of the researches focus on the influences of discharge environmental parameters, such as the types of discharge gas,[7,12] gas flow rate,[13] ratio of fuel to oxidizer (e.g., equivalence ratio, mixture ratio),[14,15] pressure and temperature,[9,12,16] on the discharge plasma and combustion control. However, in the aspect of discharge operating parameters, especially the actuating frequency of an alternating current-dielectric barrier discharge (AC-DBD),[17,18] the relevant researches are still quite insufficient compared with the discharge environmental parameters. As one of the advantages of PAC, an active adjustment can be made easily through changing the discharge actuating frequency to realize an optimal effect on combustion control according to the practical situation. Considering these facts, it is very necessary to investigate the influence of the actuating frequency on the PAC process.

With increasing enthusiasm and demand for hypersonic vehicles, a detonation engine which has a very high combustion efficiency and a fast energy release rate has become one of the best candidates for hypersonic propulsion systems.[1,19] As is well known, the difficulty that restricts the application of detonation engines is how to initiate the detonation wave fast enough over a short distance. Considering the many merits of nonequilibrium plasma assisted combustion technology, some researchers recently tried to initiate the detonation wave by dielectric barrier discharge plasma. Compared with traditional spark discharge which produces thermal equilibrium plasma, dielectric barrier discharge and corona discharge which generate nonequilibrium plasma have shown great potential in detonation initiation. For example, it was found that the ignition delay of transient plasma ignition (TPI) technology is 5 ms shorter than that of an automobile spark plug in the detonation initiation experiments of stoichiometric aviation kerosene-air mixture,[20,21] in which the TPI is a kind of dielectric barrier discharge. Several detonation initiation experiments also showed that TPI is able to reduce the ignition delay notably in either a quiescent or a mobile flow.[22] Focusing on the detonation initiation by nanosecond DBD plasma assisted, Starikovskiy[15] *et al.* pointed out that the discharge energy can be deposited into the desired internal degrees of

*Project supported by the Open Project of Science and Technology on Scramjet Laboratory, China (Grant No. CG-2014-05-118) and the National Natural Science Foundation of China (Grant No. 91441123).

†Corresponding author. E-mail: nws1969@126.com

© 2018 Chinese Physical Society and IOP Publishing Ltd

freedom of molecules through adjusting the reduced electric field, and in the PAC process containing air, the most promising active species are O atoms. A comparison of PAC dynamics among different C_2-hydrocarbons in shock wave tube experiment leads to the conclusion that the type of fuel has a strong effect on the efficiency of nonequilibrium excitation for ignition and combustion control.[23] Moreover, the influence of the equivalence ratio on plasma assisted detonation initiation under lean burn conditions has been studied in our preceding work,[24] and it showed that lowering the equivalence ratio will have an adverse effect on the benefits of plasma.

The main objective of this paper is to understand how nonequilibrium plasma generated by AC-DBD affects the detonation formation process at different actuating frequencies. Based on the establishment of an AC-DBD plasma model and a plasma-combustion model, the detonation initiation of a premixed hydrogen–oxygen gas assisted by the plasma is numerically investigated. The distributions of discharge products, flow field characteristics of the detonation tube at several typical moments, histories of thrust wall pressure, and deflagration-to-detonation transition (DDT) times and distances are all obtained and analyzed in detail under different actuating frequencies.

2. Models and methods

2.1. Simulation of discharge

The DBD configuration is depicted in Fig. 1. A high voltage electrode is located at $y = 0$ mm and a grounded electrode is located at $y = 10$ mm, with a dielectric layer covering on its surface (the thickness of the dielectric layer is assumed to be zero). Thus, the discharge gap has a size of $d_G = 10$ mm. The discharge varies only along the y direction to establish a one-dimensional (1D) model (the discharge is uniform in the x direction as we ignore the edge effect and others). The gap is filled with a premixed stoichiometric hydrogen–oxygen mixture at an initial pressure of 1.0 atm (1 atm = 1.01325×10^5 Pa), and at a temperature of 500 K.

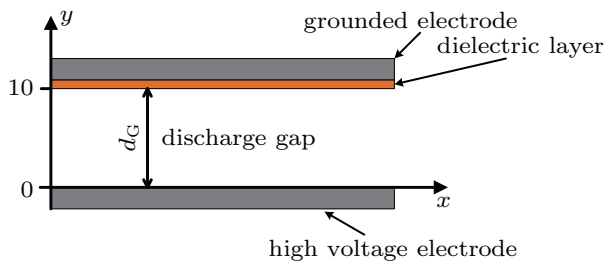


Fig. 1. (color online) Schematic diagram of discharge simulation configuration.

The governing equations for discharge simulation consist of the drift-diffusion equations for positively charged, negatively charged, and neutral particles, and Poisson's equation for the electric field as follows:

$$\frac{\partial n_k}{\partial t} + \nabla\left(\mu_k n_k \boldsymbol{E}\right) - \nabla^2\left(D_k n_k\right) = S_k, \tag{1}$$

$$\frac{\partial n_k}{\partial t} - \nabla\left(\mu_k n_k \boldsymbol{E}\right) - \nabla^2\left(D_k n_k\right) = S_k, \tag{2}$$

$$\frac{\partial n_k}{\partial t} - \nabla^2\left(D_k n_k\right) = S_k, \tag{3}$$

$$\frac{\partial^2 \phi}{\partial y^2} = -\frac{e}{\varepsilon_0 \varepsilon_d}\sum Z_k n_k, \tag{4}$$

where n_k is the number density of particle k; μ_k and D_k denote the mobility and diffusion coefficients respectively; S_k is the reaction source term; φ, e, ε_0, and ε_d are the electric potential, elementary charge, permittivity of free space, and relative permittivity, respectively; $\varepsilon_d = 3.0$; n_k and Z_k are the number density and charge of particle k, respectively. Then, the strength of the electric field is calculated by the following equation:

$$\boldsymbol{E} = -\nabla\phi. \tag{5}$$

A total of 47 discharge elemental reactions[25] are used where the positively charged particles O^+, O_2^+, H_2^+, H^+, negatively charged particles O^-, O_2^-, O_3^-, OH^-, and neutral particles O, O_2, O_3, H_2, H, OH, H_2O are taken into account. Boundary conditions are expressed as $n_k = 0$ (for negative charged particles) and $\partial n_k/\partial y = 0$ (for positive charged particles) at the high voltage electrode, $\phi = 0$ V at the grounded electrode, and $\partial n_k/\partial y = 0$ at the surface of the dielectric layer. The particle velocity at the electrode surface is limited in practice, yet the boundary conditions used here lead to an infinite velocity value of particle, so the distributions of species concentration are given by fitting functions, which are determined based on the overall distributions excluding the several values near the electrode boundary.

The DBD actuator is driven by a sinusoidal AC power supply and the frequencies of 8 kHz, 10 kHz, and 12 kHz are selected for comparison, while the voltage is fixed at 14 kV. The selected actuating frequencies are in the range of the commonly used frequencies in our AC-DBD experiments. A quasi-neutral plasma cloud is used as the initial condition; the number densities of O_2^+ and electrons are both 10^{15} m^{-3} initially in the entire domain, while other species are assumed to be zero.

Poisson's equation is discretized by the central differential method and the successive over relaxation (SOR) approach is utilized. The Crank Nicolson-finite element method (CN-FEM) is used to solve the drift-diffusion equations. The convective and diffusion terms are evaluated by the upstream scheme and central differential scheme, respectively. The spatial and temporal computational grid sizes are 5 μm and 0.02 ns, respectively. Details concerning the equations, reaction mechanisms, boundary and initial conditions, together with the numerical solving schemes can be found in Ref. [25].

2.2. Simulation of detonation initiation

Based on the obtained discharge results, an arrangement of electrode, which is compatible to the discharge simulation in the first stage, is put forward for the detonation tube as shown in Fig. 2. The entire computational domain of reaction flow is a cylinder tube with an axial length of 800 mm. The inner diameter is 23 mm with a discharge gap size of 10 mm. The closed side wall, also called the thrust wall of a detonation combustor, is on the left end of the tube and the outlet is at the right end. A rod shaped high voltage electrode is connected to the center of the closed side wall with an axial length of 10 mm and an outer diameter of 3 mm. The cylindrical wall of the detonation tube is set to be the grounded electrode directly with a dielectric layer covering its internal surface, and the axial length of the grounded electrode is also 10 mm. To restrict the discharge region between the two electrodes (this domain is called "the discharge space"), insulating material is adopted for the other part of the wall. For simplicity, the discharge is assumed to be uniform along the axial and circumferential directions with neglecting the influence of curvature on the spatial electric field, which is generally acceptable as reported in Refs. [26] and [27], so the former discharge results can be used in the later simulation. For easy comparison, the computational configuration stays unchanged when the DBD actuator is turned off, and the traditional heat ignition is performed within the discharge space for all cases.

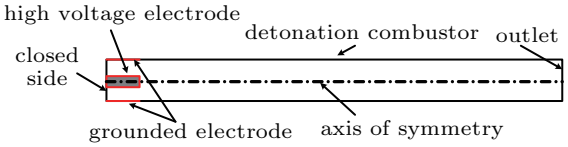


Fig. 2. (color online) Computational domain and electrode arrangement.

The loosely-coupled approach is used to deal with the simulation of plasma assisted detonation initiation here.[25,28] According to the operation sequence, that is, the first step is to start the discharge and the second step is to perform the heat ignition, the spatial distributions of key radicals and molecules at the moment when all the radicals reach their relatively high concentrations, which is obtained in the first stage (i.e., discharge simulation), together with the widely used traditional heat ignition,[29] are chosen as the initial conditions of the second stage (i.e., combustion simulation) in the discharge space.

Structural meshes are adopted in the whole computational domain. One mesh scheme that consists of 839 800 cells is chosen, with the minimum grid step being 0.1 mm. An axisymmetric boundary is specified for the axis of the detonation tube, so the total mesh cell number is half of the above-mentioned original mesh cell number. When the outflow is subsonic, the local static pressure is set to be 1 atm at the outlet and all other variables are extrapolated from the upstream zone; when the outflow is supersonic, a supersonic extrapolation condition is assumed here. The species is assumed to be air at the boundary. No slip and adiabatic conditions are imposed on the entire wall of the tube. The tube is filled with stoichiometrically mixed quiescent hydrogen and oxygen with an initial temperature of 500 K and a pressure of 1.0 atm. The heat ignition zone, which is adjacent to the closed side wall, has a temperature of 3000 K and an axial length of 10 mm.

The unsteady Reynolds averaged Navier–Stokes equations together with the realizable k–ε turbulence model, chemical source term, and multi-species conservation equations are solved as reaction flow governing equations. The finite rate reaction model is used for combustion simulation, and the 6-species 7-reaction scheme is selected as the O_2–H_2 chemical kinetic model. The dynamic processes of detonation wave formation and its propagation are both well captured by the simulation program, and details about related equations, physical models, solving methods, and validation can be found in Refs. [25] and [30].

3. Results and discussion

Since the most direct effect of adjusting the actuating frequency is a change in the plasma properties, the distribution characteristics of the discharge products are analyzed. It has been pointed out in Section 2 that the distributions of discharge products must be obtained before simulating the process of plasma assisted detonation initiation. Thus, two aspects including the discharge and detonation formation are studied respectively in the subsection below.

3.1. Temporal and spatial characteristics of discharge products

In order to study the influences of the actuating frequency on the temporal and spatial distribution of discharge plasma, three frequencies including $f = 8$ kHz (Case 1), $f = 10$ kHz (Case 2), and $f = 12$ kHz (Case 3) are chosen. The temporal and spatial distributions of the number density of key active radicals O, H, and electrons in the 4th discharge cycle T for the three cases are shown in Fig. 3. It is found that the frequency does not change the pattern of the distribution of every particle basically, yet it changes the magnitude of number density. The density of every particle declines as the frequency rises from 8 kHz to 12 kHz. This should be attributed to the fact that a higher actuating frequency means a shorter duration of single discharge, leading to a decrease in the ionization degree. Furthermore, atom O is the most sensitive to the variation of frequency according to the relative change of the peak value of particle density. Specifically, the maximum density of Case 3 is reduced by about 43.3% compared with Case 1. As for the other two particles, it is found that only the electron density decreases in constant amplitude as the frequency rises continuously.

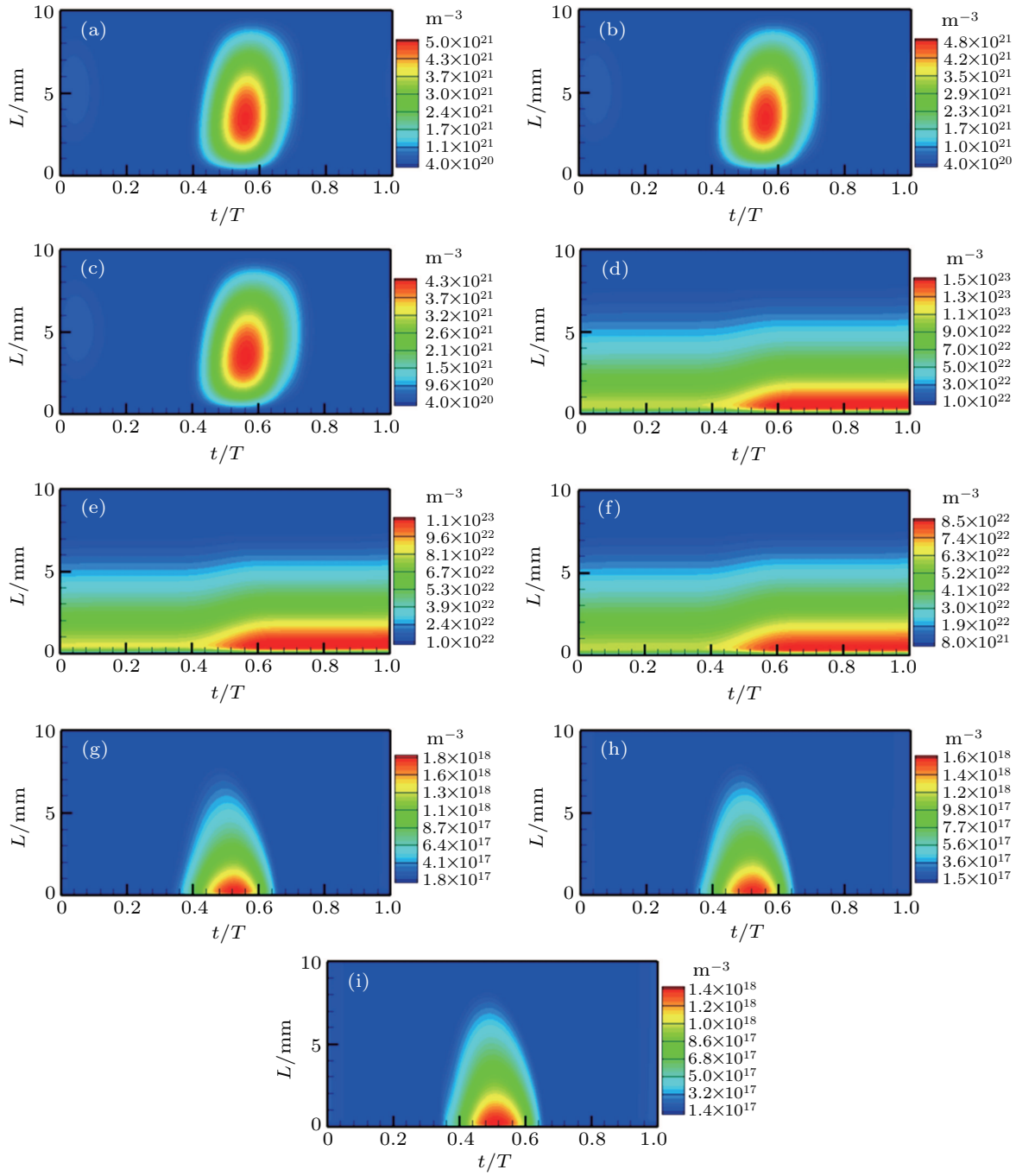


Fig. 3. (color online) Temporal and spatial distributions of discharge products. (a) $f = 8$ kHz, H, (b) $f = 10$ kHz, H, (c) $f = 12$ kHz, H, (d) $f = 8$ kHz, O, (e) $f = 10$ kHz, O, (f) $f = 12$ kHz, O, (g) $f = 8$ kHz, electron, (h) $f = 10$ kHz, electron, (i) $f = 12$ kHz, electron.

The reason for the concentration of active species decreasing as the actuating frequency rises is related to the discharge power, which can be determined by the following equation:

$$P = \frac{\sum_{i=1}^{n} U_i I_i}{n}, \tag{6}$$

where U_i and I_i are the voltage and the current at the i-th moment, n is the total number of moments of one cycle.

As shown in Table 1, the discharge power decreases as frequency rises in a nonlinear manner. When other discharge environmental and actuator control parameters are kept unchanged, the energy input into the plasma will increase with a larger discharge power. This will benefit the break of the species chemical locks, such as chemical bonds, then more active particles are formed.

Table 1. Relationship between actuating frequency and discharge power.

f/kHz	8	10	12
P/W	14.9	12.8	11.1

Among all the intermediate species of the discharge

plasma, radicals O, H, and OH have notably higher number densities than the others in the simulation results (other intermediate species are not presented here). It has been reported[1,31] that it is the three species that have relatively high concentrations in a hydrogen-oxygen discharge plasma, and have the strongest influence on ignition under the given conditions. Therefore, only species O, H, and OH are considered in the combustion simulation. In view of the fact that nearly all of the three key radicals reach their highest concentration at about $t = 0.6T$ based on the temporal and spatial distributions of their density for every case, the concentration distributions of O, H, OH, H_2, and H_2O at $0.6T$ are therefore selected as the initial conditions of subsequent combustion simulations, while other species with low concentration are ignored except for O_2.

3.2. Detonation initiation process

As is well known, the whole DDT process consists of five sub-processes, which are of the very slow combustion right after ignition, deflagration with a rising burn velocity, over-driven detonation, decay of over-driven detonation, and propagation of self-sustain stable detonation. Three flow statuses including the static, subsonic, and supersonic exist in the detonation tube during a DDT history. Thus, both the flow field at typical moments and the whole history of flow evolution are required for comparison and analysis.

3.2.1. Before the formation of stable detonation waves

Figure 4 shows the distributions of Mach numbers in the detonation tube at two typical moments $t = 70$ μs and $t = 100$ μs. These two moments are selected because they reflect the flow behaviors at the subsonic stage and the supersonic stage, respectively, before a stable detonation wave forms, and it is easy to distinguish the wave front from a Mach number distribution at the moments. The flow field structures of the three cases which have different actuating frequencies are almost the same at a certain moment. The flow is still in subsonic state at $t = 70$ μs yet it reaches supersonic at $t = 100$ μs. It is found that the wave front becomes close to the thrust wall for the given moments as the frequency rises from 8 kHz to 12 kHz by comparing the x positions of the leading wave in the panels, indicating that the DDT process develops slower as the frequency rises, however the change is very small.

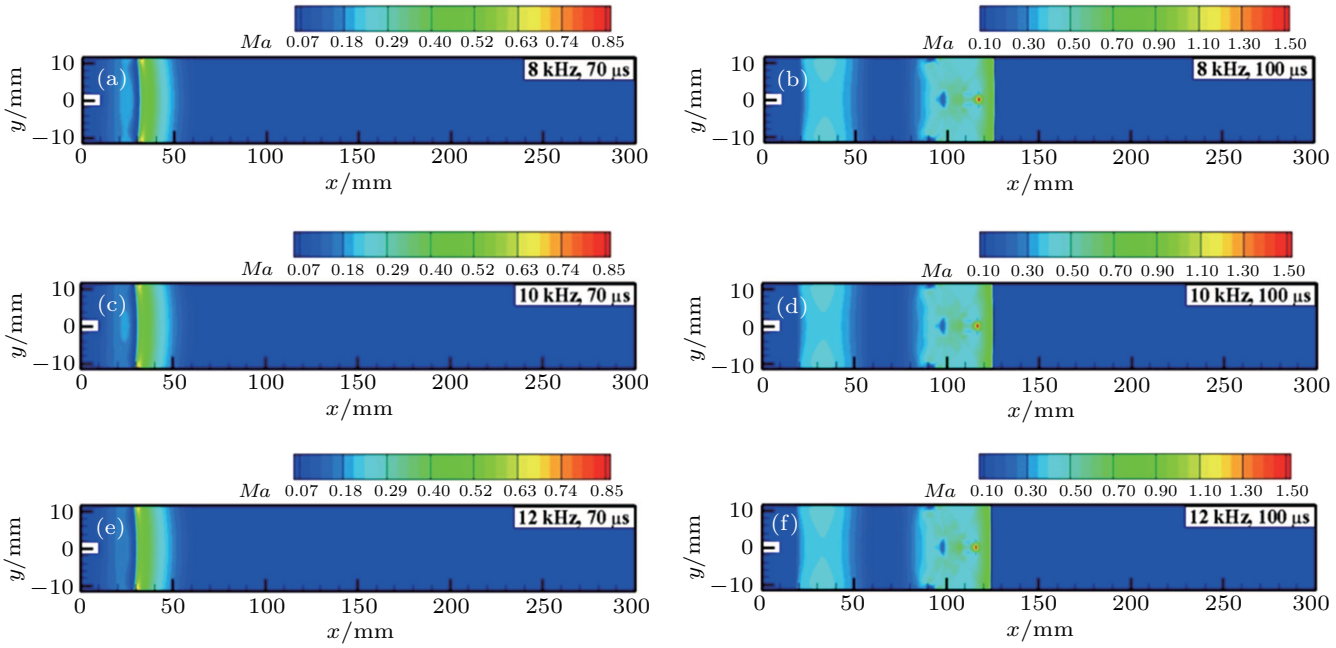


Fig. 4. (color online) Mach number distributions in detonation tube under different frequencies. (a) $f = 8$ kHz, $t = 70$ μs, (b) $f = 8$ kHz, $t = 100$ μs, (c) $f = 10$ kHz, $t = 70$ μs, (d) $f = 10$ kHz, $t = 100$ μs, (e) $f = 12$ kHz, $t = 70$ μs, (f) $f = 12$ kHz, $t = 100$ μs.

To realize the accumulated variation led by the plasma during the whole subsonic phase, the profiles of pressure, temperature, and species concentration along the tube axis at $Ma = 1$ are presented in Fig. 5. An x range covering the abrupt changing curves of flow field parameters is selected here. Like the description of the flow structures in Fig. 4, none of the overall profile characteristics of each parameter are changed by the frequency at $Ma = 1$. Only the positions of the leading shock waves of the three cases are different. Specifically, the leading shock wave in the $f = 12$ kHz case moves farthest away from the thrust wall, the next is the $f = 10$ kHz case, and the last is the $f = 8$ kHz case. The fine differences can be distinguished from Fig. 5(c) clearly: the distances in x-direction between every two adjacent steep curves, which represent the reaction boundary, are both about 0.4 mm.

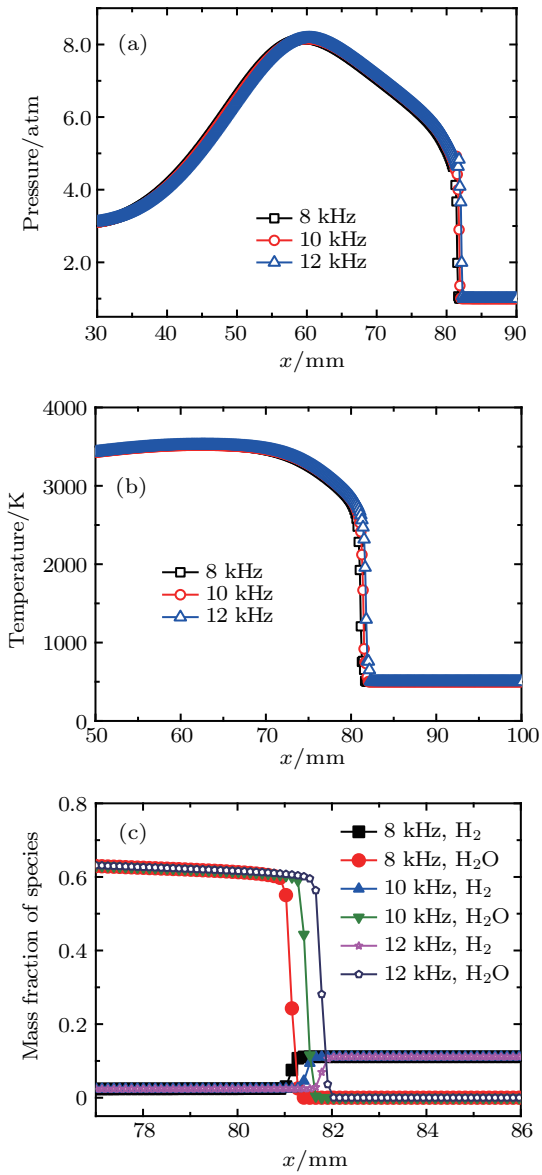


Fig. 5. (color online) Profiles of flow field parameters along the x axis at Ma=1 under different frequencies: (a) pressure, (b) temperature, (c) mass fraction of H_2 and H_2O.

3.2.2. DDT time and distance, and steady propagation stage

Figure 6 shows plots of DDT time and distance versus actuating frequency, which are received from the profile of the flow field parameter along the x axis at the moment when the Chapman–Jouguet (CJ) detonation wave has just formed. It is clear that the time and distance required for the stable detonation wave forming increase as frequency rises. The change caused by the frequency rising from 10 kHz to 12 kHz is notably larger than that caused by the frequency rising from 8 kHz to 10 kHz. Specifically, the former is about 3.9 times the τ_{DDT} of the latter, and it is about 4.9 times the L_{DDT} of the latter, indicating that the DDT time and distance increase in a non-constant amplitude way, though the frequency rises in an equal amplitude.

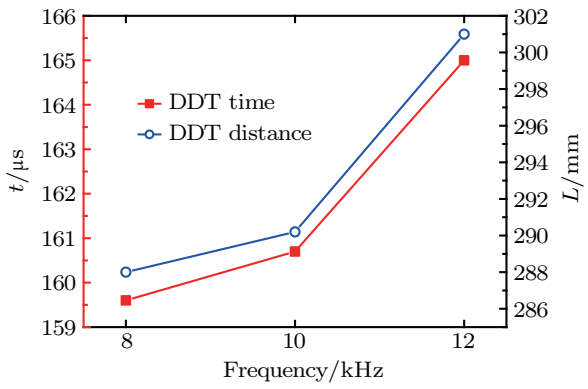


Fig. 6. (color online) Plot of DDT time and distance versus frequency.

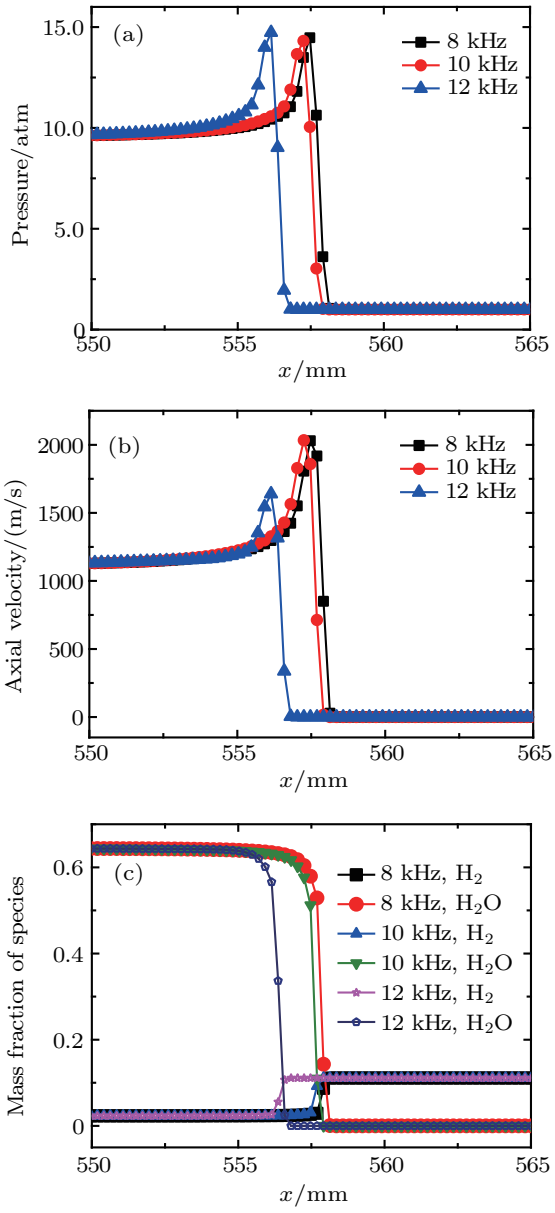


Fig. 7. (color online) Profiles of flow field parameters along the x axis at t = 260 μs under different frequencies: (a) pressure, (b) axial velocity, (c) mass fraction of H_2 and H_2O.

To further realize the effect of actuating frequency on the propagation of a stable detonation wave, the profiles of pressure, axial velocity, and species concentration along the tube

axis at $t = 260$ μs are shown in Fig. 7 for the three cases. At this moment, the abruptly changing curves of the flow parameters become steeper than those of Fig. 5, and the peak values of pressure profiles, especially the profiles of the mass fraction of H_2 and H_2O, are higher.

In accordance with the detonation initiation orders (i.e., the DDT time and distance) of the three cases, the detonation wave of the lowest frequency ($f = 8$ kHz) case moves farthest at this moment, the next is the $f = 10$ kHz case, and the last is the $f = 12$ kHz case. In addition, the length relationship of the distance between two adjacent leading shock waves among the three cases also accords with the length relationship of the DDT distance, that is, the wave front of the $f = 12$ kHz case lags behind a lot, while the interval of the wave front between the $f = 8$ kHz case and the $f = 10$ kHz case is very narrow. Compared with the positional relationships among the wave fronts of these cases at the moment when a stable detonation wave has not yet formed (as shown in Fig. 5), the distance between the $f = 12$ kHz case and the other two cases is elongated notably, so the positional relationships of the wave front at the three frequencies are changed after the completion of the detonation initiation. In summary, the effect of the actuating frequency on the detonation forming process varies in the five sub-processes.

3.2.3. History of thrust wall pressure

Due to the close correlation between the thrust wall pressure and the performance of detonation engine, and the prominent unsteady characteristics of the pressure, it is necessary to study the dynamic characteristics of the pressure on the thrust wall.

Figure 8 shows the history of thrust wall pressure under different actuating frequencies. Here, the thrust wall refers to the inner closed side wall of the tube excluding the surface of the central electrode, and the magnitude of the pressure is an area weighted average value. Generally, the frequency seems to have no influence on the history. The pressure eventually tends to a steady value after a remarkable summit. According to the magnification of the highest pressure summit, the $f = 8$-kHz case reaches its maximum value first, the next is the $f = 10$-kHz case, and the last is the $f = 12$-kHz case. From the time span shown in the magnification graph, we can see that the flow field is still in the detonation evolution phase, and the axial differences among the three cases are nearly the same, which are in accordance with the above mentioned results about the influence of frequency on flow field evolution before a stable detonation wave is formed. As for the amplitudes of pressures, there is no difference among them. Thus, it is assumed that the actuating frequency does not affect the amplitude of thrust wall pressure.

Based on the analysis above, it is concluded that a relatively low actuating frequency makes it faster to initiate the detonation, and the influence of frequency on the flow field evolution varies with time nonuniformly. However, the amplitudes of a certain flow field parameter are almost identical for different frequencies in the whole evolution process.

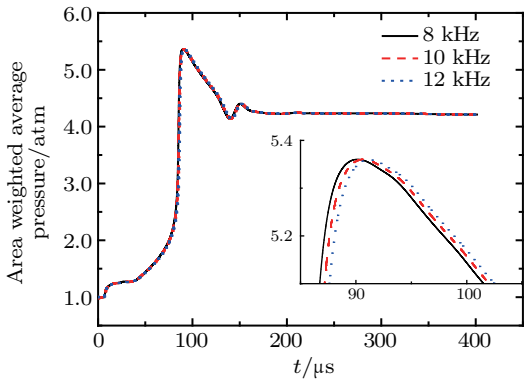


Fig. 8. (color online) Histories of pressure on thrust wall under different frequencies.

4. Conclusions

Based on the establishment of an alternating current dielectric barrier discharge model and a plasma assisted detonation initiation model, the influences of actuating frequency on the discharge products and the detonation forming process are numerically studied. Results show that the pattern of the distribution of the discharge product will basically be unchanged by adjusting the actuating frequency, yet the number density of every active particle declines as the actuating frequency rises, and the frequency has the strongest influence on atom O. Through checking the discharge powers of the three cases, it is found that the power decreases as the frequency rises, which is adverse to the generation of active species. For the adopted three actuating frequencies, the DDT time and distance both increase unevenly as the frequency rises at constant amplitude. It is inferred from comparing the positions of leading waves at different moments, that the effects of the actuating frequency during the detonation forming phase and the steady propagation phase are different. Moreover, the change of the actuating frequency does not affect the magnitude of the flow field parameter or the thrust wall pressure.

Acknowledgment

The authors wish to thank Mr. Daniel R Churchman for improving the language in this paper.

References

[1] Starikovskiy A and Aleksandrov N 2013 *Prog. Energy Combust. Sci.* **39** 61
[2] Nie W S, Zhou S Y and Che X K 2017 *High Voltage Eng.* **43** 1749 (in Chinese)
[3] Ju Y and Sun W 2015 *Prog. Energy Combust. Sci.* **48** 21
[4] Zhou S, Nie W, Che X 2015 *IEEE Trans. Plasma Sci.* **43** 896
[5] Cathey C D, Tang T, Shiraishi T, Urushihara T, Kuthi A, Gundersen M A 2007 *IEEE Trans. Plasma Sci.* **35** 1664

[6] Vincent-Randonnier A, Larigaldie S, Magre P and Sabel'nikov V 2007 *Plasma Sources Sci. Technol.* **16** 149

[7] Tang J, Zhao W and Duan Y 2011 *Plasma Sources Sci. Technol.* **20** 045009

[8] Versailles P, Chishty A W and Vo D H 2012 *J. Eng. Gas Turbines Power* **134** 031501

[9] Rakitin A, Nikipelov A and Starikovskiy A 2013 51*st AIAA Aerospace Science Meeting including the New Horizons Forum and Aerospace Exposition,* January 7–10, 2013, Grapevine, Texas, USA, p. 1054

[10] Nagaraja S, Yang V, Yin Z and Adamovich I 2014 *Combust. Flame* **161** 1026

[11] Ju Y, Lefkowitz J K, Reuter C B, Won S H, Yang X, Yang S, Sun W, Jiang Z and Chen Q 2016 *Plasma Chem. Plasma P* **36** 85

[12] Uddi M, Guo H, Sun W and Ju Y 2011 49*th AIAA Aerospace Science Meeting including the New Horizons Forum and Aerospace Exposition*, January 4–7, 2011, Orlando, Florida, USA, p. 970

[13] Liu X J, He L M, Yu J L and Zhang H L 2015 *Chin. Phys. B* **24** 045101

[14] Sun W, Uddi M, Won S H, Ombrello T, Carter C and Ju Y 2012 *Combust. Flame* **159** 221

[15] Starikovskiy A, Aleksandrov N and Rakitin A 2012 *Philos. Trans. R. Soc. A* **370** 740

[16] Ouyang J M, Shao F Q and Zou D B 2011 *Acta Phys. Sin.* **60** 110209 (in Chinese)

[17] Shao T and Yan P 2015 *Atmospheric Gas Discharge and Application of Discharge Plasma* (Beijing: Science Press) p. 163 (in Chinese)

[18] Shao T, Wang L, Zhang C, Zhou Y, Han L, Xu X and Schamiloglu E 2016 *IEEE Trans. Plasma Sci.* **44** 2072

[19] Phylippov Yu G, Dushin V R, Nikitin V F, Nerchenko V A, Korolkova N V and Guendugov V M 2012 *Acta Astronaut.* **76** 115

[20] Busby K, Corrigan J, Yu S, Williams S, Carter C, Schauer F, Hoke J, Cathey C and Gundersen M 2007 45*th AIAA Aerospace Sciences Meeting and Exhibit*, January 8–11, 2007, Reno, Nevada, USA, p. 1028

[21] Lefkowitz J K, Guo P, Ombrello T, Won S H, Stevens C A, Hoke J L, Schauer F and Ju Y 2015 *Combust. Flame* **162** 2496

[22] Cathey C, Wang F, Tang T, Kuthi A, Gundersen A M, Sinibaldi O J, Brophy C, Barbour E, Hanson K R, Hoke J, Schauer F, Corrigan J and Yu J 2007 45*th AIAA Aerospace Sciences Meeting and Exhibit*, January 8–11, 2007, Reno, Nevada, USA, p. 443

[23] Kosareva I N, Kindyshevaa S V, Momota R M, Plastinina E A, Aleksandrova N L and Starikovskiy A Yu 2016 *Combust. Flame* **165** 259

[24] Zhou S, Nie W, Che X, Chen Q and Zhang Z 2017 *Aerosp. Sci. Technol.* **69** 504

[25] Zhou S, Wang F, Che X and Nie W 2016 *Phys. Plasmas* **23** 123522

[26] Shcherbanev S A, Lepikhin N D, Klochko A V, Stepanyan S A, Popov N A and Starikovskaia S M 2015 53*rd AIAA Aerospace Science Meeting*, January 5–9, 2015, Kissimmee, Florida, USA, p. 412

[27] Pendleton S J 2012 "An Experimental Investigation by Optical Methods of the Physics and Chemistry of Transient Plasma Ignition", Ph. D. Dissertation (Los Angeles: University of Southern California)

[28] Han J and Yamashita H 2014 *Combust. Flame* **161** 2064

[29] Yan C and Fan W 2005 *Theory and Key Technology of Pulsed Detonation Engine* (Xi'an: Northwestern Polytechnical University Press) pp. 12–18 (in Chinese)

[30] Zhou S, Nie W and Che X 2016 *Combust. Sci. Technol.* **188** 1640

[31] Lan Y, He L, Ding W and Wang F 2010 *Acta Phys. Sin.* **59** 2617 (in Chinese)